J. Fluid Mech. (1989), *vol.* 201, *pp.* 279–298
Printed in Great Britain

The linear stability of mixed convection in a vertical annulus

By L. S. YAO AND B. B. ROGERS
Department of Mechanical and Aerospace Engineering, Arizona State University, Tempe, AZ 85287, USA

(Received 17 December 1987 and in revised form 2 October 1988)

The linear stability characteristics of non-isothermal flow in vertical annuli has been determined for two geometries. The analysis demonstrates that a fully developed mixed-convection flow in a vertical annulus is unstable in certain regions of an appropriate parameter space. Consequently, parallel countercurrent flows, predicted by previous numerical models and commonly used by engineers, are often physically unrealizable and can be observed experimentally only in special circumstances. In addition, it is found that the most unstable disturbances are often asymmetric in the parameter range of practical interest. The instability behaviour was also found to depend on whether the inner or outer cylinder was heated.

1. Introduction

Non-isothermal flows in ducts are of fundamental importance in engineering applications. Unfortunately, understanding of this motion and the associated heat-transfer mechanisms is incomplete and, in fact, often erroneous. An example of this lack of understanding is often found in the analysis of fully developed, mixed-convection flows in ducts. Fully developed *isothermal* flow is characterized by a constant axial pressure gradient, with the transverse velocity components equal to zero. Hence, fully developed isothermal flow is a *parallel* flow. Mixed convection results when temperature gradients in the forced flow lead to density gradients in the fluid and, in the presence of a gravitational field, these variations in density induce varying body forces in the fluid. In this situation, it is still common to model the flow as being parallel. When this assumption is made the velocity and temperature profiles become easily predicted functions of the transverse variables only, and the problem is greatly simplified. However, a consequence of this simplification is that physically unrealistic parallel reverse flows are predicted. Regrettably, many correlations for heat transfer and pressure drops in ducts have been developed from these simple, but erroneous, results. It is the purpose of this paper to demonstrate that parallel flow in a heated vertical annulus is unstable in most regions of the appropriate parameter space so that a parallel flow in such a duct will seldom be observed experimentally.

Since the annular configuration is commonly used in engineering applications, a complete understanding of the non-isothermal flow in such geometries is important. In addition, from a computational standpoint, the annular configuration allows investigation of a wide range of geometrical effects. For example, in the narrow-gap limit the problem approaches that of flow in an infinite two-dimensional slot. As the gap width is increased, the effects of wall curvature become important. In this paper, the linear stability of fully developed, mixed-convection flow in annuli of moderate

aspect ratio, in which the effects of wall curvature are quite significant, is investigated.

It has been demonstrated that flow in a heated horizontal annulus behaves quite differently from the corresponding isothermal flow. Secondary flows induced by the density stratification completely alter the flow transition and heat-transfer mechanism, and the flow can certainly not be considered to be parallel (Nieckele & Pantakar 1985; Kaviany 1986). With a vertical annulus, the effect of the density variation on the flow is not as obvious. It will be demonstrated, however, that, because of hydrodynamic instability, the flow in a vertical annulus will, in many cases, not be a parallel flow.

Several investigators have obtained numerical and analytical results for mixed convection in vertical annuli (e.g. Shumway & McEligot 1971; El-Shaarawl & Sarhan 1980; Kim 1985; Hashimoto, Akino & Kawamura 1986). These results were based on the use of the parallel-flow assumption. Consider, however, the results of Maitra & Raju (1975), who developed an exact solution for the Nusselt number based on parallel, fully developed flow in an annulus, with a constant heat flux on the inner wall and an adiabatic outer wall, and compared their analytical result to experiment. They found that the measured heat-transfer rates were significantly higher than those predicted by the theoretical model. This effect occurred at Reynolds numbers as low as 200. It is speculated by Maitra & Raju, correctly we believe, that the discrepancy between theory and experiment was due to hydrodynamic instabilities. Careful experimental observations of the flow patterns of non-isothermal flows in annuli are not available.

A related problem which has been studied more extensively is non-isothermal flow in a vertical pipe. An extensive list of pertinent references can be found in Zeldin & Schmidt (1972). Most studies have adopted the assumption of parallel flow in their analysis. Important exceptions include the work of Scheele & Hanratty (1962), who observed experimentally that the flow in a heated circular tube is stable near the inlet, but becomes unstable near the fully developed region. When buoyancy forces oppose the motion of the fluid, such as in upward flow in a cooled pipe, the transition to turbulence is abrupt. However, when they aid the motion of the fluid, the initial transition results in a new laminar equilibrium non-parallel flow. Thus, in the opposing-flow case, the instability is subcritical, and in the aided-flow case it is supercritical. Flow patterns for the supercritical case were observed by Kemeny & Somers (1962), and were called *non-laminar* to distinguish them from fully turbulent flow. The non-laminar heat-transfer rates were found to be as much as 30% larger than those observed in laminar flow. In addition, it was found that the flow can become non-laminar at Reynolds numbers as low as 30. Analytical confirmation of these results was achieved by Yao (1987*a*), who demonstrated that upward flow in a heated vertical pipe is unstable for certain parameters and that a supercritical instability will likely consist of a double-spiral structure. A stability analysis by Yao (1987*b*) for opposing mixed convection in a vertical pipe demonstrates similar behaviour.

In this paper, a linear stability analysis of fully developed, non-isothermal flow in a vertical annulus is performed. Although the stability of non-isothermal flow in a vertical annulus has not been previously investigated, a number of studies, relevant to the present investigation, will be briefly reviewed. Three limiting cases of the present study are readily identified: (i) the narrow-gap limit is analogous to a two-dimensional channel flow; (ii) the problem approaches the free-convection limit as the Reynolds number Re approaches zero; and (iii) the flow becomes isothermal as

the Grashof number Gr goes to zero. In addition, combinations of these limiting conditions result in other situations which have previously been studied. In particular, isothermal flow in a narrow-gap annulus approaches plane Poiseuille flow, while free convection in such an annulus approaches free convection in an infinite, two-dimensional vertical slot.

The linear stability of plane Poiseuille flow has received a great deal of attention. Early work used involved asymptotic methods. Numerical solutions are now routine and show that the flow is unstable at a Reynolds number, based on slot width and average velocity, of about 7700.

The problem of the stability of natural convection in an infinite two-dimensional vertical slot has also received considerable attention. The original work was done by Gershuni (1953), who used a Galerkin method (at the lowest order of approximation possible) to study the stability of natural convection between infinite vertical plates maintained at different temperatures. The accuracy of the method was later refined by including more terms in the approximation by Gershuni & Zhukhovitskii (1955) and Rudakov (1967). Birikh (1966) studied the hydrodynamic stability of plane parallel flows with cubic velocity profiles. Such a situation arises in natural convection of a fluid of zero Prandtl number contained between infinite vertical plates maintained at different temperatures. Addressing the problem of minimizing heat transfer between vertical boundaries, Gill & Davey (1969) developed a stability criterion for air in a infinite slot based on the slot width and the temperature difference between the surfaces. Birikh *et al.* (1969) investigated the effect of a longitudinal temperature gradient imposed on the transverse temperature difference. Vest & Arpaci (1969) investigated the problem both analytically and experimentally. In their analysis it is shown that, for a basic state possessing odd symmetry and disturbances expanded in the classical normal-mode form, the disturbance wave speed must be zero. It is pointed out by Gill & Kirkham (1969) that this result is not completely general, and results are presented which show that, at large Prandtl number, the instability sets in as travelling waves. However, at larger values of Pr, the disturbance energy can originate from the potential energy associated with the buoyant forces. Korpela, Gozum & Chandrakant (1973) addressed this dependence on the Prandtl number and found that, at Prandtl numbers below 12.7, the disturbances are stationary.

The stability of natural convection in tall vertical annuli has been investigated by Choi & Korpela (1980) and McFadden *et al.* (1984). Choi & Korpela investigated only axisymmetric disturbances and found that the instability boundary is a function of the aspect ratio and Prandtl number. For air, they found that the critical Grashof number varied from about 8000 in the limit of a two-dimensional slot to about 14000 in a slot with an aspect ratio of 0.25. At smaller aspect ratios, the critical Grashof number for an axisymmetric disturbance became large. McFadden *et al.* (1984) extended these results to account for azimuthal modes. Their results showed that, for air, at an aspect ratio of about 0.77 and critical Grashof number of about 9500, the most unstable disturbance becomes the first circumferential mode. The value of the critical Grashof number is approximately 10000 for all aspect ratios smaller than 0.79.

Mott (1966) determined the stability boundary, based on axisymmetric disturbances, for isothermal flow in an annulus for several aspect ratios using asymptotic methods, and verified his results with finite-difference calculations. He found that as the aspect ratio decreased the value of the critical Reynolds number increased. Mott & Joseph (1968) expand these results and discuss the possibility of

asymmetric disturbances being important. In each case, however, only axisymmetric disturbances are investigated.

The assumption that the most unstable disturbance will be axisymmetric in the case of annular flows is quite restrictive. Squire's theorem, which is valid for two-dimensional flows, states that the growth rate of an unstable three-dimensional wave is equal to that of a two-dimensional wave at a smaller Re. Consequently, stability studies on plane Poiseuille flow are usually limited to two-dimensional disturbances. This result can also be derived for the problem of natural convection in a two-dimensional slot (Vest & Arpaci 1969). However, an analogue of Squire's theorem cannot be proved rigorously for an axisymmetric basic flow. In spite of this, many investigators have assumed that the disturbances of interest are axisymmetric in their studies. On the other hand, McFadden *et al.* (1984) found that the most unstable disturbance for natural convection in annuli is asymmetric at small aspect ratios. Further indication of this phenomenon is found in the results of Yao (1987*a*, *b*) which show that heated flow in a vertical pipe first becomes unstable to asymmetric disturbances over a large portion of the parameter domain. The conclusions mentioned above make it clear that a complete determination of the linear stability boundary will require investigation of asymmetric disturbances.

A linear-stability analysis of fully developed flow in a vertical annulus, with one surface maintained at a temperature a constant amount above the other, is performed in the next section. The analysis accounts for both axisymmetric and general disturbances. The results presented are for two aspect ratios in order to demonstrate the effect of wall curvature. The outcome shows that the flow is unstable (see figures 4 and 5) for certain parameter ranges. In addition, it is found that the most unstable disturbances are often asymmetric.

2. Problem formulation

Consider the annular geometry illustrated in figure 1. If we define a dimensionless radial coordinate as $\eta = (r-b)/(a-b)$ and an aspect ratio as $A = b/(a-b)$, where a and b are, respectively, the outer and inner radii of the cylinders, the dimensionless Navier–Stokes and energy equations, in terms of annular-cylindrical coordinates (η, ϕ, z) are

$$\frac{\partial u}{\partial \eta}+\frac{u}{\eta+A}+\frac{1}{\eta+A}\frac{\partial v}{\partial \phi}+\frac{\partial w}{\partial z}=0, \tag{1a}$$

$$\frac{\partial u}{\partial t}+\mathrm{D}_1 u-\frac{v^2}{\eta+A}=-\frac{\partial P}{\partial \eta}+\frac{1}{Re}\left[\mathrm{D}_2^2 u-\frac{1}{(\eta+A)^2}\left(2\frac{\partial v}{\partial \phi}+u\right)\right], \tag{1b}$$

$$\frac{\partial v}{\partial t}+\mathrm{D}_1 v+\frac{uv}{\eta+A}=-\frac{1}{\eta+A}\frac{\partial P}{\partial \phi}+\frac{1}{Re}\left[\mathrm{D}_2^2 v+\frac{1}{(\eta+A)^2}\left(2\frac{\partial u}{\partial \phi}-v\right)\right], \tag{1c}$$

$$\frac{\partial w}{\partial t}+\mathrm{D}_1 w=-\frac{\partial P}{\partial z}+\frac{1}{Re}[\mathrm{D}_2^2 w]+\frac{Gr}{Re^2}\theta, \tag{1d}$$

$$\frac{\partial \theta}{\partial t}+\mathrm{D}_1 \theta=\frac{1}{Re\,Pr}\mathrm{D}_2^2 \theta, \tag{1e}$$

where

$$\mathrm{D}_1 = u\frac{\partial}{\partial \eta}+\frac{v}{\eta+A}\frac{\partial}{\partial \phi}+w\frac{\partial}{\partial z}, \tag{2a}$$

and

$$\mathrm{D}_2^2 = \frac{\partial^2}{\partial \eta_2}+\frac{1}{\eta+A}\frac{\partial}{\partial \eta}+\frac{1}{(\eta+A)^2}\frac{\partial^2}{\partial \phi^2}+\frac{\partial^2}{\partial z^2}. \tag{2b}$$

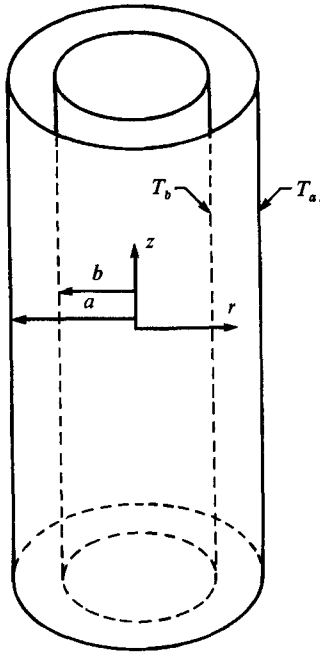

FIGURE 1. Geometry and coordinates.

The z-coordinate is non-dimensionalized by the gap width $a-b$, the velocities by the mean axial velocity W, the pressure by ρW^2, and the time by $(a-b)/W$. The dimensionless temperature is given by $\theta = (T-T_a)/(T_b-T_a)$, where T_a and T_b are the outer and inner wall temperatures, respectively. The parameters appearing in the equations are the Reynolds number $Re = (a-b)\,W/\nu$, Prandtl number $Pr = \nu/\alpha$, and the Grashof number $Gr = \beta g(a-b)^3\,(T_b-T_a)/\nu^2$, where g is the gravitational acceleration, β the thermal expansion coefficient, α, here, the coefficient of thermal diffusivity, and ν the viscosity.

Investigation of the governing equations and their subsequent non-dimensionalization reveals that if $T_b > T_a$, Gr is positive; if $T_a > T_b$, the outer cylinder temperature is higher than that of the inner cylinder, and the only change that occurs in the governing relations is that Gr changes sign. Further investigation of the problem reveals that there are two distinct base-flow situations that may occur. These are upward flow with the outer cylinder heated (which is analogous to downward flow with the inner cylinder heated) and upward flow with the inner cylinder heated (which is analogous to downward flow with the outer cylinder heated). Therefore, by investigating the stability behaviour for both positive and negative values of Gr, the complete stability boundary for mixed convection in an annulus of a particular geometry is determined.

In this paper, two geometries are investigated. Their aspect ratios are $A = 2.414$, which corresponds to equal cross-sectional areas for the inner and outer annular regions, and $A = 10$. The larger aspect ratio was chosen to clearly illustrate the effect of wall curvature on the results. In both cases, the results will show that curvature has a significant effect on the shape of the neutral stability boundary.

2.1. *Basic state*

Since we are interested in studying the stability of non-isothermal, fully developed flow in an annular region, we split the dependent variables in the governing equations into two parts: basic state and disturbance. If the classical assumption of fully developed flow is applied to (1*a–e*), the basic state is independent of the axial and azimuthal coordinates. The governing equations are

$$\frac{Gr}{Re^2}\Theta - \frac{\partial P}{\partial z} + \frac{1}{Re}\left[\frac{\partial^2 W}{\partial \eta^2} + \frac{1}{\eta + A}\frac{\partial W}{\partial \eta}\right] = 0, \tag{3a}$$

$$\frac{\partial^2 \Theta}{\partial \eta^2} + \frac{1}{\eta + A}\frac{\partial \Theta}{\partial \eta} = 0. \tag{3b}$$

The axial-pressure gradient can be determined with the use of the requirement of global mass conservation:

$$\int_0^1 (\eta + A)\, W \, \mathrm{d}\eta = \tfrac{1}{2}(1 + 2A). \tag{3c}$$

The solutions of (3*a–c*) are algebraically complicated and are not presented here. Typical basic velocity profiles are given in figure 2. For $Gr/Re = 80$ and -80, the velocity profiles contain points of inflection which suggest a potential for instability. The corresponding basic temperature distributions are given in figure 3.

2.2. *Disturbance*

The linear equations governing the infinitesimal disturbances are obtained by subtracting the basic-state equations from the full equations and neglecting nonlinear terms. They are

$$\frac{\partial \hat{u}}{\partial \eta} + \frac{\hat{u}}{\eta + A} + \frac{1}{\eta + A}\frac{\partial \hat{v}}{\partial \phi} + \frac{\partial \hat{w}}{\partial z} = 0, \tag{4a}$$

$$\frac{\partial \hat{u}}{\partial t} + W\frac{\partial \hat{u}}{\partial z} = -\frac{\partial \hat{P}}{\partial \eta} + \frac{1}{Re}\left[\mathrm{D}_2^2 \hat{u} - \frac{\hat{u}}{(\eta + A)^2} - \frac{2}{(\eta + A)^2}\frac{\partial \hat{v}}{\partial \phi}\right], \tag{4b}$$

$$\frac{\partial \hat{v}}{\partial t} + W\frac{\partial \hat{v}}{\partial z} = -\frac{1}{\eta + A}\frac{\partial \hat{P}}{\partial \phi} + \frac{1}{Re}\left[\mathrm{D}_2^2 \hat{v} - \frac{\hat{v}}{(\eta + A)^2} + \frac{2}{(\eta + A)^2}\frac{\partial \hat{u}}{\partial \phi}\right], \tag{4c}$$

$$\frac{\partial \hat{w}}{\partial t} + \hat{u}\frac{\partial W}{\partial \eta} + W\frac{\partial \hat{w}}{\partial z} = -\frac{\partial \hat{P}}{\partial z} + \frac{1}{Re}\mathrm{D}_2^2 \hat{w} + \frac{Gr}{Re^2}\hat{\theta}, \tag{4d}$$

$$\frac{\partial \hat{\theta}}{\partial t} + \hat{u}\frac{\partial \Theta}{\partial \eta} + W\frac{\partial \hat{\theta}}{\partial z} = \frac{\hat{1}}{RePr}\mathrm{D}_2^2 \hat{\theta}. \tag{4e}$$

The continuity equation is satisfied by the choice of two stream functions, f and g, which are defined by

$$\hat{v} = \frac{\partial \hat{g}}{\partial \eta}, \tag{5a}$$

$$\hat{u} = -\left(\frac{\partial \hat{f}}{\partial z} + \frac{1}{\eta + A}\frac{\partial \hat{g}}{\partial \phi}\right), \tag{5b}$$

$$\hat{w} = \frac{\partial \hat{f}}{\partial \eta} + \frac{\hat{f}}{\eta + A}. \tag{5c}$$

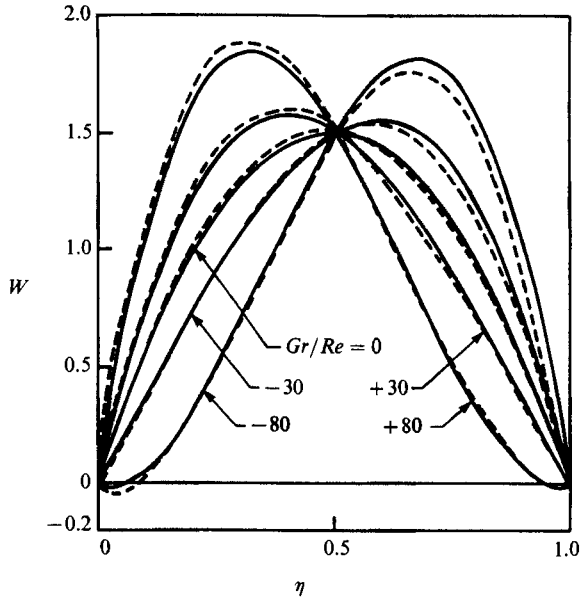

FIGURE 2. Basic-state velocity profiles. Dashed line represents $A = 2.414$, solid line $A = 10$.

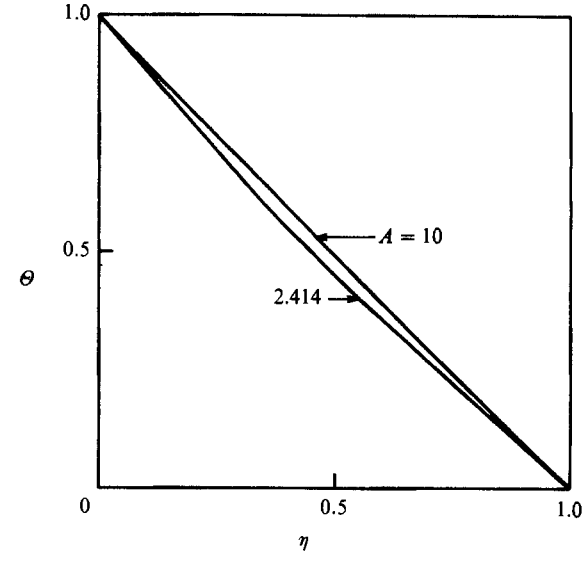

FIGURE 3. Basic-state temperature profiles.

The remaining four equations can be reduced to three by the elimination of pressure through cross-differentiation. The number of independent variables is then reduced to one with the assumption that the disturbances are of the usual normal-mode form

$$\hat{\phi} = \phi(\eta)\, e^{i[\alpha(z-ct)+n\phi]}, \tag{6}$$

where $\hat{\phi} = \hat{f}$, $\hat{g}$ or $\hat{\theta}$, and α and n are the axial and azimuthal wavenumbers, respectively. Equations (4*a–e*) then become

$$f'''' + \frac{2}{\eta+A}f''' + \left[-2\alpha^2 - \frac{(3+n^2)}{(\eta+A)^2} - \mathrm{i}\alpha Re\, W\right]f''$$
$$+\left[-2\alpha^2 + \frac{(3+n^2)}{(\eta+A)^2} - \mathrm{i}\alpha Re\, W\right]\frac{f'}{\eta+A} + \left[\frac{2\alpha^2+\alpha^2n^2}{(\eta+A)^2} + \frac{3n^2-3}{(\eta+A)^4} + \alpha^4\right.$$
$$\left. + \mathrm{i}\alpha Re\left(\frac{W}{(\eta+A)^2} + \alpha^2 W + W_{\eta\eta} - \frac{W_\eta}{\eta+A}\right)\right]f$$
$$+\left(\frac{-n\alpha}{\eta+A}\right)g'' + \left[\frac{-n\alpha}{(\eta+A)^2} + \mathrm{i}n Re\frac{W_\eta}{\eta+A}\right]g' + \left[\frac{n^3\alpha}{(\eta+A)^3}\right.$$
$$\left. + \frac{\alpha^3 n}{\eta+A} + \mathrm{i}\,Re\left(\frac{\alpha^2 n}{\eta+A}W + \frac{nW_{\eta\eta}}{\eta+A} - \frac{nW_\eta}{(\eta+A)^2}\right)\right]g + \frac{Gr}{Re}\theta'$$
$$= \mathrm{i}\alpha Re\, c\left[-f'' - \frac{1}{\eta+A}f' + \left(\frac{1}{(\eta+A)^2} + \alpha^2\right)f + \frac{\alpha n}{\eta+A}g\right], \tag{7a}$$

$$nf''' + \frac{2n}{\eta+A}f'' + \left[-\frac{n^3+n}{(\eta+A)^2} - \alpha^2 n - \mathrm{i}\alpha n\, re\, W\right]f'$$
$$+\left[-\frac{3\alpha^2 n}{\eta+A} - \frac{n^3-n}{(\eta+A)^3} + \mathrm{i}\alpha n Re\left(-\frac{W}{\eta+A} + W_\eta\right)\right]f + (-\alpha(\eta+A))\,g'''$$
$$-\alpha g'' + \left[\alpha^3(\eta+A) + \frac{\alpha+\alpha\eta^2}{\eta+A} + \mathrm{i}\alpha^2 Re\, W(\eta+A)\right]g'$$
$$+\left[-\frac{2n^2\alpha}{(\eta+A)^2} + \mathrm{i}n^2 Re\frac{W_\eta}{\eta+A}\right]g + n\frac{Gr}{Re}\theta$$
$$= \mathrm{i}\alpha Re\, c\left[-nf' - \frac{n}{\eta+A}f + \alpha(\eta+A)\,g'\right], \tag{7b}$$

$$\theta'' + \frac{1}{\eta+A}\theta' + \left[-\frac{n^2}{(\eta+A)^2} - \alpha^2 - \mathrm{i}\alpha Re\, Pr\, W\right]\theta$$
$$+ [\mathrm{i}\alpha Re\, Pr\, \Theta_\eta]f + \left[\mathrm{i}n Re\, Pr\frac{\Theta_\eta}{\eta+A}\right]g = -\mathrm{i}\alpha c\, Re\, Pr\,\theta, \tag{7c}$$

where a prime denotes differentiation with respect to η.

These equations represent a ninth-order system. Eight boundary conditions, which reflect the no-slip, no penetration and constant-temperature conditions on the inner and outer cylinders, are given by

$$g'(0) = \alpha f(0) + \frac{n}{A}g(0) = f'(0) + \frac{f(0)}{A} = \bar{\theta}(0) = 0, \tag{8a}$$

$$g'(1) = \alpha f(1) + \frac{n}{1+A}g(1) = f'(1) + \frac{f(1)}{1+A} = \bar{\theta}(1) = 0. \tag{8b}$$

The ninth boundary condition establishes a datum for the stream functions and is given by

$$g(0) = 0. \tag{8c}$$

Equations (6*a–c*) and the boundary conditions form a complex eigenvalue problem. The stability boundary in the (Re, Gr, n, α)-space is determined by the point at which the imaginary component of the complex wave speed c_i is equal to zero, with the disturbance being unstable for c_i greater than zero. This also forms a minimax problem with $c_i = 0$ where Re and Gr/Re are local minima for various wavenumbers α and n. A large number of calculations is required to establish the projection of the stability boundary on the (Gr/Re, Re)-plane. The computational method is described in the next section.

3. Method of solution

A pseudospectral Chebyshev method is used to discretize the equations and incorporate the boundary conditions (Orszag 1971). The collocation points are selected to be the extrema of the nth-order Chebyshev polynomials so that the truncation error is minimized. The eigenvalues of the resulting matrix are determined with the aid of a complex QR algorithm as described by Moler & Stewart (1973).

The convergence of the numerical scheme has been checked by varying the number of collocation points. It has been found that 51 terms are usually sufficient. For large values of the azimuthal wavenumber, more terms are needed to avoid spurious roots. It was observed that 'true' roots always appear when the number of discretization terms is increased. On the other hand, spurious roots usually appear as a group and their values change drastically when N is altered. A great deal of care was exercised to ensure that the correct eigenvalues were identified.

The accuracy and validity of the numerical scheme was checked by favourable comparison with published results in the limiting cases mentioned earlier: (i) plane Poiseuille flow; (ii) natural convection in a two-dimensional slot; (iii) natural convection in a tall annulus; and (iv) isothermal flow in an annulus.

To compare our results with those of a two-dimensional channel, we set $A = 1000$. In this case, as $Gr \to 0$, the basic flow approaches plane Poiseuille flow. In a careful numerical study of this problem, Orszag (1971) found the wave speed of the most unstable disturbance at $Re = 13333$, $\alpha = 2.0$ and $n = 0$. Our calculation of this parameter agrees with his result to 5 significant figures.

With $A = 1000$, as $Re \to 0$ the situation becomes that of natural convection between infinite parallel plates maintained at different temperatures. Lee & Korpela (1983) have determined that the critical point lies at $Gr = 8038$ and $\alpha = 2.8$. Using a linear interpolation of the imaginary component of the complex wave speed between its value at $Gr = 8000$ and 8100 at wavenumbers of $\alpha = 2.7$, 2.8, and 2.9, then using a quadratic interpolation in α of these results, we find the critical condition to be $Gr = 8015$ at $\alpha = 2.8$, a difference in the critical Grashof number of about 0.3%. The critical wave speed which we predict at this condition is $c_r \approx 10^{-5}$. This is consistent with the results of Korpela *et al.* (1973) for natural convection in a two-dimensional slot, in which it is found that for Prandtl number less than 12.7, the disturbances are stationary.

Our results for natural convection in a tall annulus can be compared to the results of Choi & Korpela (1980) and McFadden *et al.* (1984). Choi & Korpela considered only axisymmetric ($n = 0$) disturbances, while McFadden *et al.* considered both axisymmetric and asymmetric disturbances. The results in each case are nearly identical

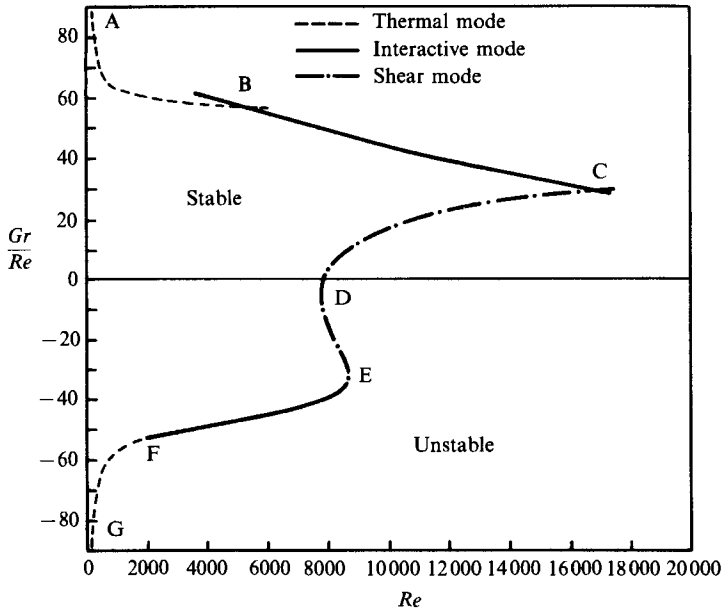

FIGURE 4. Marginal-stability boundary for $A = 10$.

when the most unstable disturbance is axisymmetric. Since the latter group considered asymmetric disturbances as well, they provide a more convenient means of comparison for our results.

At a Prandtl number of 0.71 and an aspect ratio of 1.5, McFadden *et al.* (1984) found that the critical condition is $Gr = 8512$, $\alpha = 2.75$, $n = 0$ and $c_r = 1.57 \times 10^{-3}$. Our corresponding values are $Gr = 8521$, $\alpha = 2.78$, $n = 0$ and $c_r = .1.6 \times 10^{-3}$. In the case of a non-axisymmetric disturbance at a Prandtl number of 0.71 and an aspect ratio of 0.25, McFadden *et al.* find $Gr = 10435$, $\alpha = 2.24$, $n = 1$ and $c_r = 3.1 \times 10^{-3}$. The present calculations yield $Gr = 10443$, $\alpha = 2.22$, $n = 1$ *and* $c_r = 3.1 \times 10^{-3}$. Thus, our results agree well with those in the reference for both axisymmetric and asymmetric disturbances. In addition, our calculations predict that the aspect ratio below which the most unstable disturbance will be asymmetric is $A = 0.77$, in agreement with McFadden *et al.*

In the limit if isothermal flow, our results agree well with those obtained by Mott (1966) for axisymmetric disturbances. However, we find that as the aspect ratio decreases, asymmetric modes become the most unstable. Below aspect ratios of about $A = 4$, we find that, depending on the geometry, azimuthal wavenumbers $n = 1$, 2, or 3 may establish the most unstable mode. For example, in the results presented in the next section, we find that at $Gr = 0$ and $A = 2.414$, the most unstable mode corresponds to $n = 2$. The critical Reynolds number for this mode is about 4% less than that for the axisymmetric mode.

4. Results and discussion

The following results are for $Pr = 0.71$ at $A = 2.414$ and 10. The instability boundaries in the (Re, Gr/Re)-plane are shown in figures 4 and 5. The axial and azimuthal wavenumbers and wave speed for selected critical conditions are listed in tables 1–4.

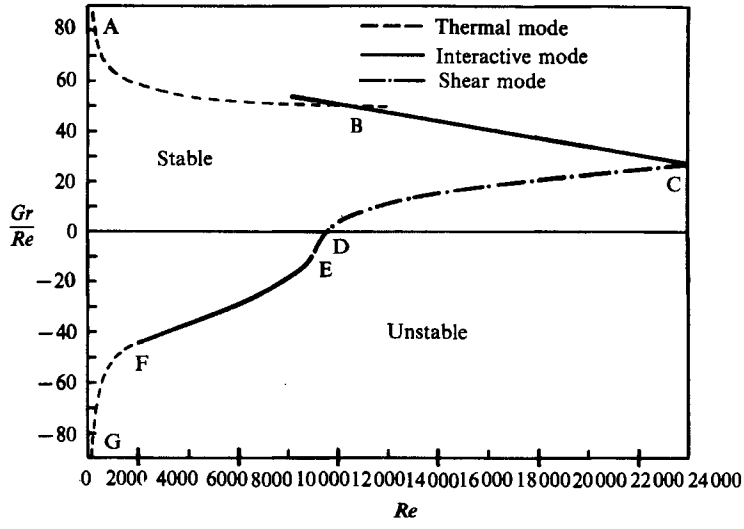

FIGURE 5. Marginal stability boundary for $A = 2.414$.

Re	*Gr/Re*	α	n	c_r	Type
150	90.57	2.53	0	0.84	T
500	68.17	2.17	8	0.71	T
1000	63.33	1.53	17	0.66	T
4000	58.05	0.86	19	0.55	T
5000	57.83	1.90	13	0.53	I
	57.83	1.83	14	0.53	I
	57.49	0.79	19	0.53	T
	57.49	0.71	20	0.55	T
6000	55.26	2.23	5	0.50	I
	55.24	2.21	6	0.50	I
	55.23	2.18	7	0.50	I
	55.23	2.25	8	0.50	I
	55.23	2.21	9	0.50	I
	55.23	2.07	10	0.50	I
	55.27	2.03	11	0.50	I
	57.07	0.75	19	0.52	T
	57.09	0.66	20	0.54	T
8000	49.47	2.25	0	0.46	I
13000	37.37	2.15	0	0.41	I
17000	30.13	2.04	0	0.37	I
7876.2	0	2.02	0	0.39	S
9000	11.97	1.97	0	0.38	S
11000	20.20	1.84	0	0.35	S
13000	24.76	1.77	0	0.34	S
15000	28.10	1.72	0	0.33	S
17000	30.26	1.68	0	0.32	S

TABLE 1. Inner wall heated, $A = 10$. T = thermal instability type; I = interactive; S = shear

Re	Gr/Re	α	n	c_r	Type
150	−89.96	2.59	0	0.79	T
500	−63.09	2.38	0	0.67	T
1000	−56.89	2.20	0	0.59	T
2000	−52.90	2.03	0	0.52	T
3000	−50.69	1.95	0	0.47	T
4000	−48.81	1.90	0	0.45	T
5000	−46.99	1.87	0	0.43	T
6000	−55.91	1.84	0	0.41	T
7000	−42.63	1.81	0	0.39	T
8000	−39.22	1.76	0	0.38	T
8500	−35.43	1.75	0	0.37	T
7876	0.0	2.02	0	0.39	S
7785	−5.0	2.02	0	0.39	S
7811	−10.0	1.98	0	0.38	S
7983	−15.0	1.95	0	0.38	S
8163	−20.0	1.88	0	0.38	S
8425	−25.0	1.84	0	0.37	S
8566	−30.0	1.78	0	0.37	S
8609	−32.5	1.77	0	0.37	S

TABLE 2. Outer wall heated, $A = 10$

Re	Gr/Re	α	n	c_r	Type
150	93.24	2.31	1	0.91	T
500	70.76	1.58	5	0.77	T
1000	63.77	1.29	5	0.68	T
3000	56.40	0.71	6	0.62	T
5000	52.79	0.70	5	0.54	T
8000	51.76	0.60	5	0.60	T
	54.28	1.29	5	0.52	I
12000	4.88	0.51	5	0.47	T
	47.60	1.42	5	0.49	I
16000	41.07	1.77	4	0.43	I
20000	34.66	1.83	3	0.39	I
24000	27.88	1.91	2	0.35	I
9530	0.0	1.87	2	0.38	S
12000	10.75	1.63	3	0.37	S
16000	18.32	1.44	3	0.35	S
20000	23.11	1.04	4	0.35	S
24000	27.29	0.94	4	0.34	S

TABLE 3. Inner wall heated, $A = 2.414$

Comparison of figures 4 and 6 reveals that the general stability behaviour in each geometry is similar. In both cases the instability boundaries behave quite differently depending on which cylinder is heated, except at low values of Re, where the results are symmetric about the $Gr = 0$ axis. Investigation of the governing relations for the basic state reveals that, in the case of natural convection ($Re = 0$), the only effect of heating the outer cylinder as opposed to the inner one is that the velocity changes sign everywhere. The only effect on the stability results is then to reverse the sign of

Re	Gr/Re	α	n	c_r	Type
150	−91.44	2.65	0	0.72	T
500	−60.12	2.45	0	0.63	T
1000	−51.42	2.27	0	0.56	T
2000	−44.48	2.09	0	0.49	I
4000	−36.62	1.94	0	0.42	I
6000	−28.89	1.88	0	0.39	I
8000	−17.01	1.83	1	0.38	I

TABLE 4. Outer-wall heated, $A = 2.414$

the disturbance wave speed. Thus, the low-Re symmetry, as the natural-convection limit is approach, is expected. For positive Gr, in both cases the effect of heat transfer is initially stabilizing (see sections denoted CDE on figures 4 and 5). In both geometries, the maximum stable values of Re are much larger than the critical Re for $Gr = 0$. Another similarity is that the regions of stable flow are much larger for positive Gr than they are for negative Gr.

In spite of the broad agreement between the results for each geometry, there are some differences in detail. For example, with the inner cylinder heated, the region of stable flow in the $(Gr/Re, Re)$-plane extends further along the Re-axis for the smaller aspect ratio than it does for $A = 10$. The points labelled C in figures 4 and 5 identify the point of maximum stable Re. With the larger aspect ratio, this point is at $Re = 16970$ for $Gr/Re = 30.22$. With the smaller aspect ratio, this value is $Re = 24200$ for $Gr/Re = 27.5$. For small Gr/Re, at $A = 10$, heating has a stabilizing effect for both positive and negative Gr (sections CD and DE on figure 4). This does not occur with the smaller aspect ratio. This indicates that, for the larger aspect ratio at small heating values, the basic state is beginning to behave like a channel flow. However, at larger heating values, even though the basic state looks very much like a two-dimensional channel flow, its stability character is different and the effect of the wall curvature is still significant. With the heated outer cylinder (negative Gr), the shape of the stability boundary is discernibly different for $A = 10$ compared to $A = 2.414$. At $A = 10$, the effect of heating is initially stabilizing, as it is with the inner cylinder heated. At $A = 2.414$ the effect of heating is always destabilizing, in contrast to results for the inner cylinder heated.

Figures 4 and 5 show that, in both cases, when the inner cylinder is heated, there are three distinct curves which form the stability boundary. The intersection between two different curves can be identified and the curves continued past the points at which they cross. This is not the case when the outer cylinder is heated. In this situation the stability boundary is formed by a single smooth curve. Because of the different character of the results, the detailed behaviour of each region is discussed separately below.

4.1. *Heated inner cylinder*

The instability that occurs at small Re will be referred to as *thermal* instability since it is induced by an unstable temperature disturbance as demonstrated by Yao (1987*a*) in the study of mixed-convection stability of vertical pipe flow. Sections AB on figure 4 and 5 identify this curve. A *shear* instability exists near $Gr = 0$, identified by sections CD on figures 4 and 5. For intermediate values, the term *iterative* instability will be used.

The above criteria for the definition of the instabilities differs from that used by Hart (1971) in which the instabilities are classified according to the source of the disturbance energy. For the *thermal* instability, a check of the energetics of the critical eigenmodes for the aspect ratio of 10 indicates that the disturbance energy is gained from both the potential energy associated with the buoyant effect and the kinetic energy associated with the Reynolds stresses. However, in this case, the kinetic energy supplies about 16 times as much energy to the disturbance as does the buoyant potential energy. This ratio is pretty much constant for the thermal mode. A check of the energetics of the critical *shear* mode for the aspect ratio of 10 indicates that the disturbance gathers about equal amounts of energy from each source. This ratio varies only slightly for the shear mode. The critical mode of the *interactive* instability at $Re = 5000$ is found to derive about 8 times as much energy from the shear forces than it does from the buoyant effect. However, with the interactive instability, at $Re = 6000$, this ratio is down to 3.6, and at $Re = 8000$, its value is 1.4. Thus, the ratio of kinetic to potential energy in the interactive instability is found to be a function of Re, and lies between the results for the thermal and shear instabilities.

Investigation of the numerical results presented in tables 1 and 3 shows that the different instabilities possess distinct characteristics. Considering first the results for $A = 10$ (table 1) it is seen that for the shear instability, $n = 0$ is clearly the most unstable mode. This behaviour is expected since, at $A = 10$, we have a nearly two-dimensional flow. The instability boundary is almost symmetric with respect to the condition $Gr = 0$ for low heating. This agrees with Squire's theorem. The wave speed c_r and the axial wavenumber α decrease with increasing Reynolds number.

For the smaller aspect ratio, the results for the shear instability in table 3 show that asymmetric disturbances are the most unstable. At $Gr/Re = 0$, $n = 2$ is the critical azimuthal mode (point D in figure 5). As Re increases, the value of the azimuthal wavenumber also increases and reaches a value of $n = 4$ *at* $Re = 24000$, near the intersection with the interactive instability boundary (point C in figure 5). The disturbance wave speed c_r and the axial wavenumber α decreases with increasing Re as they do for the larger aspect ratio.

At $A = 10$, in contrast to the shear mode, most thermal instabilities are asymmetric. The critical azimuthal wavenumber varies from $n = 0$ near the natural-convection limit to $n = 19$ near the intersection of the thermal and interactive instability boundaries (along section AB on figure 4). Because there are so many azimuthal modes that must be considered in this region, a large number of computations was necessary to establish this boundary. Minimum points for each value of n at a particular Re were determined by a quadratic interpolation of the three most unstable calculated points in the $(\alpha, Gr/Re)$-plane. This procedure did not firmly establish a single critical value for n, however. Further complication results from the fact that the critical value of the azimuthal wavenumber n is not always obvious, as is illustrated in figure 6 and table 1 for $Re = 5000$. In spite of these difficulties, the trend in the results is clear. For the thermal mode, the critical azimuthal wavenumber increases with increasing Reynolds number. As the Reynolds number increases to a value of 5000, the critical value of n increases to 19. Referring to figure 4, along section AB of the instability boundary, the critical axial wavenumber α decreases from 2.53 to 0.79 as Re increases. This indicates that the axial wavelength grows with the basic-state flow speed as is the case with the shear instability discussed above. Results for smaller Re than are presented in table 1 show that the computed critical wavenumber approaches the natural-convection critical

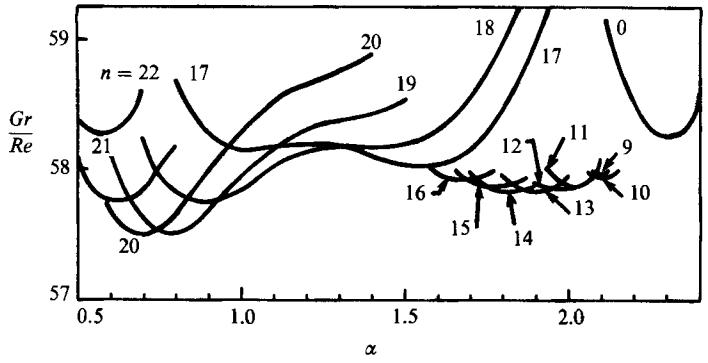

FIGURE 6. Instability behaviour in the (α, Gr/Re)-plane for $A = 10$, $Re = 5000$.

wavenumber 2.8 as $Re \to 0$. This further demonstrates the numerical accuracy of the solution method.

With the smaller aspect ratio the behaviour is similar. Referring to figure 5, along section AB of the instability boundary the critical azimuthal wavenumber n increases from 1 to 5. However, n never reaches the large values that occur with $A = 10$. This is expected since the annular gap width to circumference ratio is much smaller in this case and hence there are fewer disturbance 'cells' contained around the perimeter of the annulus. The critical axial wavenumber α again decreases with increasing Re, as it does with the larger aspect ratio. This trend is the same as that for $A = 10$, but the wave speed itself is higher than that for the larger aspect ratio. Vest & Arpaci (1969) have shown that, in the limit of natural convection in a two-dimensional channel, disturbances of the type considered here are stationary. Since buoyant forces play a dominant role in the thermal instability, as Re decreases and the aspect ratio increases, a decrease in the disturbance wave speed is not unexpected.

In between the thermal and the shear instabilities, the instability boundary possesses characteristics that distinguish it, even in regions near the intersections with the other instability boundaries, and is labelled as *interactive* in figures 4 and 5 (sections BC of the instability boundaries in figures 4 and 5). Figure 6 illustrates the appearance of two distinct minimum points in the (α, Gr/Re)-plane at $A = 10$ and $Re = 5000$. These minimum points correspond to the thermal and interactive instabilities. With the larger aspect ratio (figure 4), the curves of the thermal and the interactive instabilities intersect near $Re = 5000$, where α and n of the interactive instability are 1.9 and 13, respectively. This indicates that the interactive wave is about half of the size of the thermal instability in the axial direction and one and a half times wider in the azimuthal direction. Linear interpolation of the results at $Re = 5000$ and 6000 shows that for $Re > 5160$, the interactive instability becomes unstable at a smaller value of Gr/Re than does the thermal instability. In contrast to the thermal instability, n decreases rapidly to zero as Re increases to 8000. For $Re > 8000$, $n = 0$ remains the most unstable mode and the azimuthal wavenumber matches that of the shear instability when the curves intersect. Near the intersection of the shear and interactive instability curves, the interactive wave is shorter in the axial direction and faster than the shear wave. The two instabilities intersect at $Re = 16970$ and $Gr/Re = 30.22$.

At the smaller aspect ratio the interactive instability becomes unstable at a smaller value of Gr/Re than does the thermal instability for $Re > 10100$, but the

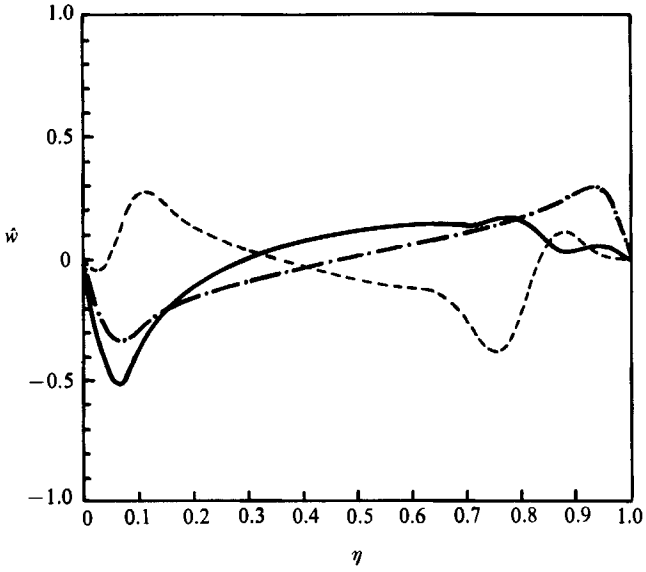

FIGURE 7. Eigenfunctions of $\hat{w}$ for $A = 10$: ----, thermal mode, $Re = 6000$, $Gr/Re = 57.07$, $\alpha = 0.75$, $n = 19$; ——, interactive mode, $Re = 6000$, $Gr/Re = 55.23$, $\alpha = 2.18$, $n = 7$; -·-·-, shear mode, $Re = 7876$, $Gr/Re = 0$, $\alpha = 2.02$, $n = 0$.

mode can be clearly identified as early as $Re = 8000$. At this point, the critical azimuthal wavenumber n is 5 and the axial wavenumber α is 1.29. In this region the thermal disturbance also has an azimuthal wavenumber of 5, but the axial wavenumber is 0.6. The wave speeds of the two instabilities are roughly equal in this region. Thus, the interactive instability can be differentiated from the thermal mode by a shorter disturbance wavelength. As Re increases, the azimuthal wavenumber decreases, until in the region of intersection with the shear-mode curve, $n = 2$. The axial wavenumber α steadily increases with increasing Re until it reaches a value of 1.91 at $Re = 24000$. The disturbance wave speed c_r decreases from 0.52 to 0.35 over this same region. At $Re = 24000$, the wavenumbers of the shear instability are $n = 4$ and $\alpha = 0.94$, and the wavespeed c_r is 0.34. Thus, the interactive instability can be identified by a small number of disturbance 'cells' around the perimeter of the annulus and a significantly shorter wavelength.

The shape of the disturbances in the radial direction can be determined from investigation of the eigenvectors for the axial disturbance velocity. Figure 7 shows mode shapes for the three identified instabilities with $A = 10$. The results for the thermal and shear instabilities at $Re = 6000$ with the inner cylinder heated show that there is a distinct difference in the mode shapes. With the thermal mode, the disturbance consists of three rotating eddies. Near the inner (heated) wall a strong eddy exists owing to the buoyant forces. The viscous action of this eddy includes the other two smaller cells. The shear instability at $Gr = 0$, shown in figure 7, consists of a single rotating eddy. The interactive mode also consists of a single rotating eddy, but in this case the streamlines are concentrated near the inner (hotter) wall.

4.2. *Heated outer cylinder*

With both aspect ratios, separate instability curves cannot be clearly identified for negative Gr (heated outer cylinder). The instability boundary can still be considered to consist of three instabilities, but the interface between them is not as obvious as

in the case of a heated inner cylinder. The instability that occurs at small Gr is the shear instability since it occurs primarily owing to the shear flow in the annulus. These instabilities form sections DE of the instability boundaries on figures 4 and 5. At small Re, the instability boundary is symmetric about the $Gr = 0$ axis with the thermal instability that occurs in the case where the inner cylinder is heated.

As previously mentioned, in the natural-convection limit, the instability boundary becomes symmetric about the $Gr = 0$ axis. Thus, the instability boundary in the region where the curves are symmetric is formed by the thermal instability, denoted by sections FG on figures 4 and 5. In between the thermal and the shear boundaries is a region where both thermal and shear-flow effects are important and the instability boundary is not symmetric about the $Gr = 0$ axis. This is the interactive instability, denoted by sections EF on figures 4 and 5.

Considering first the large aspect ratio, at small Gr/Re the shear instability is nearly symmetric with respect to $Gr = 0$. Although the influence is less pronounced for negative Gr, in both cases heating has a stabilizing effect. For a heated outer cylinder, the maximum stable Re is 8610 at $Gr/Re = -32.5$. Similar to the case of a heated inner cylinder, the critical n is zero, and the shear wave speed and axial wavenumbers decrease with increasing Re.

In the larger-aspect-ratio case, the thermal instability possesses many characteristics identified previously for positive Gr. A comparison of the results in tables 2 and 4 shows that, at $Re = 150$, the critical Gr/Re are almost identical. At $Re = 1000$, the difference has increased to about 10%. As Re increases, α and c_r decrease, which agrees with the general trend of the thermal instability identified for positive Gr.

The interactive instability also behaves in a manner analogous to the case for the inner cylinder heated. Referring to figure 4, proceeding from point F toward point E, this curve initially forms approximately a straight line. The slope of this line is about equal to the negative of the slope of the corresponding line for positive Gr. The azimuthal wavenumber n is zero throughout this range.

In spite of the similarities discussed above between the cases of the inner-cylinder and outer cylinder heated, significant differences can be identified. The first is that, in the case of the heated outer cylinder, the different modes blend together in a smooth fashion and only one instability can be identified in the intersecting region. Secondly, in contrast to the case of a heated inner cylinder, the most unstable disturbance for the thermal mode is always axisymmetric ($n = 0$). Another major difference is the shape of the instability boundary. The stabilizing effect of heat transfer on the shear instability is much greater in the case of the heated inner cylinder.

In the case of the smaller aspect ratio, figure 5 reveals no symmetry around the $Gr/Re = 0$ axis. Thus the boundary between the interactive and shear instabilities is less obvious than it was in the case of the larger aspect ratio. It is still possible, however, to identify these instabilities. In the region where Gr/Re is small, the stability boundary is formed by a curve with a larger slope than the curve forming the boundary at larger heating values (section DE on figure 5). The break in the curve occurs at about $Re = 8000$ and $Gr/Re = -10$. Thus, even though a shear instability can be identified for this case, its region of influence is relatively small. At small Re, symmetry is again observed about the $Gr = 0$ axis. However, in this case the symmetry is confined to very small Re. For example, at $Re = 150$, the critical values of Gr/Re for the inner and outer cylinder heated cases are 93.24 and -91.44, respectively. At $Re = 500$, however, these values are 70.76 and -60.12, a difference

of more than 10%. Hence, the region of influence of the thermal instability is also quite small in this case, and most of the instability boundary in the lower half-plane is formed by the interactive instability, section EF in figure 5.

With the smaller aspect ratio, it is again seen that the interactive instability possesses some general characteristics similar to the corresponding instability that occurs with a heated inner cylinder. For example, α, c_r and the critical value of Gr/Re decrease with increasing Re. However, in this case the numerical results are significantly different than those for positive Gr. The magnitude of Gr/Re at which the flow becomes unstable is much less with the outer cylinder heated. For instance, at $Re = 8000$, the critical Gr/Re with a heated inner cylinder occurs are 54.28; with a heated outer cylinder, this value is -17.01. The wave speed is also slower with the heated outer cylinder. In contrast to the results for a heated inner cylinder, n for this case is zero for Re between 150 and 6000. However, at $Re = 8000$, $n = 1$ has become the most unstable mode, and at the intersection with the $Gr = 0$ axis, $n = 2$ is the critical mode. Thus, the shear-instability disturbances are not axisymmetric. However, over most of the region, the thermal and interactive instability disturbances are axisymmetric, as they are with the larger aspect ratio.

5. Conclusions

It has been demonstrated that mixed convection in a vertical annulus is unstable in a large portion of an appropriate parameter space. This suggests that parallel mixed-convection flows with reverse-flow regions are unlikely to be observed experimentally, except possibly at very low Re. Heat-transfer correlations developed from numerical techniques that assume laminar flow without considering flow instability are likely to give very poor results.

The marginal stability boundary is found to be formed by three types of instabilities. At low speeds, the thermal instability is dominant. At higher speeds and low heating, the flow becomes unstable to a shear instability. In between these cases is the interactive instability.

The shape of the marginal stability boundary in the ($Re/Gr/Re$)-plane depends on whether the inner or outer cylinder is heated. With the inner cylinder heated, the boundary is formed by three distinct curves which can be easily differentiated from one another by the different wavenumbers and wave speeds of each instability. In particular, the thermal instability is characterized by a larger axial wavelength and higher disturbance wave speed than those of the interactive instability in the regions near the intersection of the curves. Near the points of intersection of the interactive and shear instabilities, the interactive instability has a smaller axial wavelength and a higher disturbance wave speed than does the shear instability. It is also found that the most unstable disturbances are very often asymmetric when the inner cylinder is heated.

With the outer cylinder heated the boundary is formed by a single smooth curve and the identification of the separate instabilities is not as obvious. The three instabilities mentioned above can still be identified, however, by investigation of the marginal stability boundary. With the outer cylinder heated, the most unstable disturbances are usually axisymmetric. The only exception to this is with an aspect ratio of 2.414 and low amounts of heating, when it is found that the first azimuthal mode ($n = 1$) is the most unstable. This result is expected however, since it is found that isothermal flow in an annulus of this aspect ratio first becomes unstable to the second azimuthal mode ($n = 2$).

REFERENCES

BIRIKH, R. V. 1966 On small perturbations of a plane parallel flow with cubic velocity profile. *Appl. Mat. Mech.* **30**, 432–438.

BIRIKH, R. V., GERSHUNI, G. Z., ZHUKHOVITSKII, E. M. & RUDAKOV R. N. 1972 On oscillatory instability of plane parallel convective motion in a vertical channel. *Appl. Math. Mech.* **33**, 707–710.

CHOI, I. G. & KORPELA, S. A. 1980 Stability of the conduction regime of natural convection in a tall vertical annulus. *J. Fluid Mech.* **99**, 725–738.

EL-SHAARAWL, M. A. I. & SARHAN, A. 1980 Free convection effects on the developing laminar flow in vertical concentric annuli. *Trans. ASME* C: *J. Heat Transfer* **102**, 617–622.

GERSHUNI, G. Z. 1953 On the stability of plane convective motion of fluid. *Zh. Tekh. Fiz.* **23**, 1838.

GERSHUNI, G. Z. & ZHUKHOVITSKII, E. M. 1958 On two types of instability of a convective flow between parallel plates. *Isv. Vyssh. Uchebn. Zavedenii Fiz.* **4**, 43.

GILL, A. E. & DAVEY, A. 1969 Instabilities of a buoyancy driven system. *J. Fluid Mech.* **35**, 775–798.

GILL, A. E. & KIRKHAM, C. C. 1970 A note on the stability of convection in a vertical slot. *J. Fluid Mech.* **42**, 125–127.

HART, J. E. 1971 Stability of the flow in a differentially heated inclined box. *J. Fluid Mech.* **47**, 547–576.

HASHIMOTO, K., AKINO, N. & KAWAMURA, H. 1986 Combined forced free laminar heat transfer to a highly heated gas in a vertical annulus. *Intl. J. Heat Mass Transfer* **29**, 145–151.

KAVIANY, M. 1986 Laminar combined convection in a horizontal annulus subject to constant heat flux inner wall and adiabatic outer wall. *Trans. ASME* C: *J. Heat Transfer* **108**, 392–397.

KEMENY, G. A. & SOMERS, E. V. 1962 Combined free and forced convective flow in vertical circular tubes – experiments with water and oil. *Trans. ASME* C: *J. Heat Transfer* **84**, 339–346.

KIM, J. H. 1985 Analysis of laminar natural convection superimposed on downward flow in a vertical tube annulus. *ASME Winter Annual Meeting* 85-WA/HT-13.

KORPELA, S. A., GOZUM, D. & CHANDRAKANT, B. B. 1973 On the stability of the conduction regime of natural convection in a vertical slot. *Intl. J. Heat Mass Transfer* **16**, 1683–1689.

LEE, Y. & KORPELA, S. A. 1983 Multicellular natural convection in a vertical slot. *J. Fluid Mech.* **126**, 91–121.

MAITRA, D. & RAJU, K. S. 1975 Combined free and force convection laminar heat transfer in a vertical annulus. *Trans. ASME* C: *J. Heat Transfer* **97**, 135–137:

MCFADDEN, G. B., CORIELL, S. R., BOISVERT, R. F. & GLICKSMAN, M. E. 1984 Asymmetric instabilities in buoyancy driven flow in a tall vertical annulus. *Phys. Fluids* **27**, 1359–1361.

MOLER, C. B. & STEWART, G. W. 1973 An algorithm for generalized matrix eigenvalue problems. *SIAM. J. Numer. Anal.* **10**, 241–256.

MOTT, J. E. 1966 Stability of viscous parallel flows in annular channels. Ph.D. dissertation, University of Minnesota.

MOTT, J. E. & JOSEPH, D. D. 1968 Stability of parallel flow between concentric cylinders. *Phys. Fluids* **11**, 2065–2073.

NIECKELE, A. O. & PANTAKAR, S. V. 1985 Laminar mixed convection in a concentric annulus with a horizontal axis. *Trans. ASME* C: *J. Heat Transfer* **107**, 902–909.

ORSZAG, S. A. 1971 Accurate solution of the Orr–Sommerfeld stability equation. *J. Fuid Mech.* **50**, 689–703.

RUDAKOV, R. N. 1967 Spectrum of perturbations and stability of convective motion between vertical plates. *Appl. Math. Mech.* **31**, 376–383.

SCHEELE, G. F. & HANRATTY, T. J. 1962 Effect of natural convection on stability of flow in a vertical pipe. *J. Fluid Mech.* **14**, 244–256.

SHUMWAY, R. W. & MCELIGOT, D. M. 1971 Heated laminar gas flow in annuli with temperature dependent transport properties. *Nucl. Sci. Engng* **46**, 394–407.

VEST, C. M. & ARPACI, V. S. 1969 Stability of natural convection in a vertical slot. *J. Fluid Mech.* **36**, 1–15.

YAO, L. S. 1987*a* Is fully-developed and non-isothermal flow possible in a vertical pipe? *Intl. J. Heat Mass Transfer* **30**, 707–716.

YAO, L. S. 1987*b* Linear stability analysis for opposing mixed convection in a vertical pipe. *Intl. J. Heat Mass Transfer* **30**, 810–811.

ZELDIN, B. & SCHMIDT, F. W. 1972 Developing flow with combined forced free convection in an isothermal vertical tube. *Trans. ASME* C: *J. Heat Transfer* **94**, 211–223.